MARCH 18 2026

Impact of viscous-grain shearing parameters on transmission loss in sediment acoustics

Aiden C. Edwards; Michelle S. Wang; Aviana Smith; Jay C. Spendlove ; Tracianne B. Neilsen; Mark K. Transtrum

Proc. Mtgs. Acoust. 54, 070007 (2024)
https://doi.org/10.1121/2.0002258

Volume 54 http://acousticalsociety.org/

Acoustics Week in Canada

Joint Meeting
186th Meeting of the Acoustical Society of America
and the Canadian Acoustical Association

Ottawa, Ontario, Canada
13-17 May 2024

Underwater Acoustics: Paper 2pUW6

Impact of viscous-grain shearing parameters on transmission loss in sediment acoustics

Aiden C. Edwards and Michelle S. Wang
Department of Physics and Astronomy, Brigham Young University, Provo, UT, 84604, USA; aidencedwards@gmail.com; eruzaprisca@gmail.com

Aviana Smith
Department of Physics and Astronomy, Idaho State University Boise, Boise, ID, USA; avianasmith@u.boisestate.edu

Jay C. Spendlove, Tracianne B. Neilsen and Mark K. Transtrum
Department of Physics and Astronomy, Brigham Young University, Provo, UT, 84602, USA; jayclark24@gmail.com; traci.neilsen@byu.edu; mktranstrum@gmail.com

One approach to investigating parameter sensitivity in seabed models is to apply the techniques of information geometry. This paper provides an information geometric analysis of a sound propagation in a shallow-water waveguide, where the acoustic properties of the sediment are derived from the viscous grainshearing (VGS) model. Specifically, we consider single-frequency transmission loss (TL) across a wide range of VGS parameters. By exploring the limits and boundaries of the TL model manifolds, particularly as parameters approach both low and high extremes, this approach allows for the determination of relative stiffness and sloppiness of model parameters and provides indications of parameter hierarchies and correlations. Results include slices of the model manifold and matrices of information distances on a fivedimensional model man-ifold, representing the absolute transmission loss at 16 receiver depths for different sediment types. Careful examination of these results provides insights into the relative impact of VGS parameters and the delineation of limiting regions. This work demonstrates how information geometry can inform model selection and parametrization in geoacoustic inversion studies, leading to more efficient and interpretable models of the seabed.

Proceedings of Meetings on Acoustics, Vol. 54, 070007 (2026); https://doi.org/10.1121/2.0002258.

1. INTRODUCTION

In the realm of complex modeling and data analysis, understanding how model parameters influence predictions is crucial. Information geometry offers a robust framework for this purpose by leveraging concepts from differential geometry and statistics, providing insights into the structure of models and the relationship between parameters and data. In particular, information geometry aids in model selection by quantifying the information content that observational data provide about model parameters. This quantification allows for the determination of which parameters are essential and should be retained in the model and which parameters add little to no modeling value and can be excluded. This approach is particularly useful in complex models where not all parameters contribute equally to the accuracy and reliability of predictions.

Within the information geometry framework, model parameters can be categorized as stiff or sloppy. Stiff parameters are those that are well-constrained by the data, meaning small changes in these parameters can lead to significant changes in model predictions. In contrast, sloppy parameters are poorly constrained, where variations in these parameters result in negligible changes in model outcomes. Sloppiness can arise either because the parameters do not significantly influence the model or because certain combinations of parameters produce similar effects, making it difficult to isolate individual parameter contributions. As such, sloppy parameters can lead to ambiguous and unreliable model interpretations. By identifying and removing sloppy parameters, reduced models are obtained without sacrificing accuracy while offering improved robustness and interpretability.

Information geometry provides many tools to visualize and quantify parameter influence. For example, the Fisher Information Matrix (FIM) helps in understanding the curvature of the parameter space, which in turn indicates how sensitive the model is to changes in each parameter. Parameters associated with high curvature regions are stiff, while those in flat regions are sloppy. In addition to the FIM, information geometry introduces the concept of a model manifold, which is the main tool used in this investigation.

In our exploration of a complex model's behavior, the model manifold serves as a geometric representation embedded within the data space. Just as the FIM provides a quantitative understanding of parameter sensitivity, the model manifold provides a visual and geometric perspective of how different parameter configurations affect the model's behavior. In this manuscript, we evaluate the model manifold for transmission loss (TL) as sound propagates through an ocean where the seabed is parameterized by the viscous grain-shearing (VGS) model.[1–3] The TL model manifold is evaluated in two way: the edge lengths of two-dimensional slices of the model manifold and the information distance on the model manifold between different seabed types. Both provide insights into the relative stiffness and sloppiness of the parameters in different regimes and provide insights into the potential advantages of creating a reduced order sediment model based on porosity.

2. METHODS

A. THE MODEL MANIFOLD

The model manifold is a way to geometrically represent and visualize a model's outputs. The model manifold for the model of a sum of two decaying exponentials model is presented in Fig. 2 to

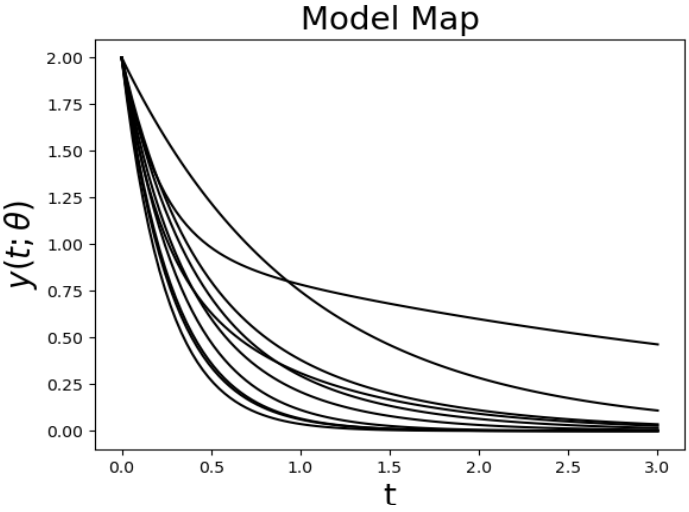

Figure 1: Model map of the sum of decaying exponentials model, with different model realizations using different values of θ.

illustrate the insights that can be gained from this approach. The sum of two decaying exponentials is written as

$$y(t;\boldsymbol{\theta}) = e^{-\theta_1 t} + e^{-\theta_2 t} \quad , \quad \theta_\mu \geq 0.$$

Often we visualize a model in terms of fixed model parameters $\boldsymbol{\theta}$ with varying independent variable t, as we do for the sum of exponentials model in Fig. 1. We could instead define the model at distinct observation points $\boldsymbol{t} = [t_1, ...t_M]$, similar to real life data which is often collected at discrete intervals (e.g., hydrophones at specific depths on a vertical line array). This is known as the model map $\boldsymbol{Y}(\boldsymbol{\theta})$:

$$\boldsymbol{Y}(\boldsymbol{\theta}) = \begin{bmatrix} y(t_1;\boldsymbol{\theta}) \\ y(t_2;\boldsymbol{\theta}) \\ \vdots \\ y(t_M;\boldsymbol{\theta}) \end{bmatrix}. \tag{1}$$

The model manifold is then constructed by calculating the model map $\boldsymbol{Y}(\boldsymbol{\theta})$ at all possible choices of $\boldsymbol{\theta}$. For the sum of decaying exponentials model, the bounds on the individual θ_μ in *parameter space* are defined as shown in the schematic of parameter space provided in Fig. 2(a), where the colored lines represent three special cases: green for when either θ_μ goes to infinity, orange for when either θ_μ goes to zero, and red for when $\theta_1 = \theta_2$. By calculating the model map $\boldsymbol{Y}(\boldsymbol{\theta})$ for each sampled $\boldsymbol{\theta}$ in Fig. 2(a) and plotting in *data space*, we obtain the model manifold, as shown in Fig. 2(b).

The model manifold can be thought of as the generalization of the column space, for a nonlinear mapping. The dimensionality of the model manifold is the same as the dimensionality of the parameter space, e.g., if you have an N-dimensional parameter space, the manifold is an N-dimensional surface embedded in an M-dimensional data space (where M is the number of observation points t_i). For this sum of exponentials model, the parameter space and model manifold

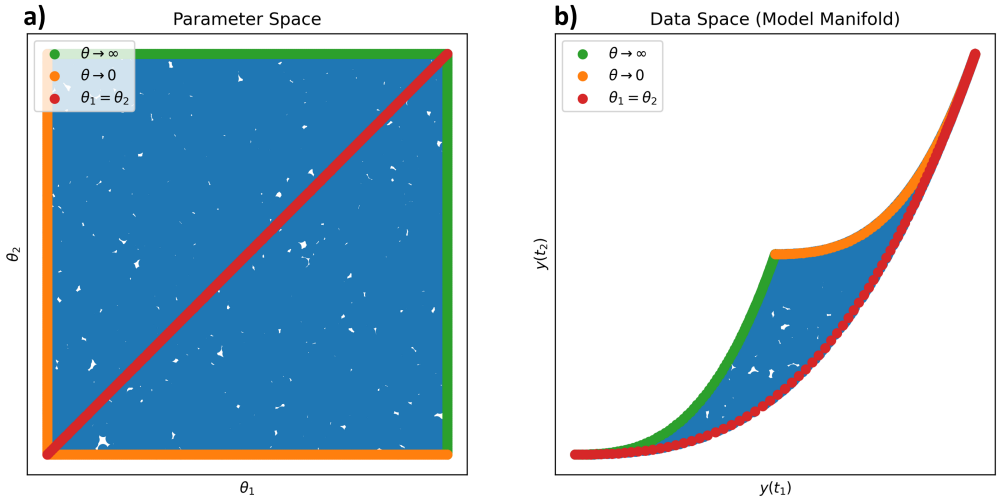

Figure 2: (a) Parameter space and (b) data space visualizations for the sum of exponentials model for two selected values of t. The model manifold is displayed for $t_1 = 1$ and $t_2 = 2$. The green boundary of the model manifold corresponds to one of the θ_μ values approaching infinity, the orange boundary corresponds to one of the θ_μ approaching 0, and the third boundary corresponds to $\theta_1 = \theta_2$.

are two-dimensional (corresponding to θ_1 and θ_2), and the data space shown is two-dimensional because two different model realizations are calculated (at times t_1 and t_2). When the data space is higher dimensional, you can take a two- or three-dimensional slice of the M-dimensional data space to visualize the manifold.

Examination of the geometry of the model manifold yields insight into parameter sensitivity and identifiability or uncertainty when the model is employed to infer $\boldsymbol{\theta}$. For complex models, some parameters are 'sloppy', or unidentifiable; these parameters are not constrained by the observed data, resulting in large parametric uncertainty. Due to the insensitivity of sloppy parameters, the model manifold is bounded and thin in some directions, indicating that the manifold has lower effective dimensionality. The boundaries often correspond to taking the sloppy parameters to limiting values, such as zero and infinity.

In the sum of exponentials case, for example, there are three boundaries on the model manifold. One boundary corresponds to taking either θ_1 or θ_2 to infinity (green), one boundary corresponds to taking θ_1 or θ_2 to 0 (orange), and the third boundary (red) corresponds to $\theta_1 = \theta_2$. This specific model manifold is symmetric about $\theta_1 = \theta_2$, because θ_1 and θ_2 can be interchanged without changing the model output. Generally, the model manifold has a unique structure that allows us to learn about the stiffness or sloppiness of the modeling parameters in $\boldsymbol{\theta}$. The next section discusses how to use the structure of the model manifold may be used to facilitate sloppy parameter recognition for sound propagation models.

B. SOUND PROPAGATION IN THE OCEAN

The ability to accurately model and predict the behavior of sound underwater is crucial for a wide range of applications. Ocean experiments contain many complexities, such as the inherent difficulty of creating experimental datasets due to the time and expense. Compared to conducting extensive experimental studies, existing sound propagation models offer efficient alternatives. Examples that are useful in shallow ocean environments include the numerical normal mode models, such as ORCA,[4] and analytical normal mode models like the Pekeris waveguide[5,6] for simplified ocean environments.

These sound propagation models numerically compute the transmission loss (TL) based on the modeling parameters in $\boldsymbol{\theta}$. TL quantifies the impact of sound propagation and represents the decrease in acoustic energy as sound waves propagate through a medium from the source to the receiver. TL accounts for energy losses due to absorption, reflection, and spreading as sound waves travel. By quantifying how much acoustic energy is lost during propagation, TL provides insights into the impact of environmental factors on acoustic signal propagation. These factors include depth, temperature, salinity of the water, and sediment properties. These sediment properties intricately affect the reflectivity and absorptivity of the seafloor.[7] Understanding the impact of sediment properties on sound propagation is essential for deriving meaningful insights from acoustic data.

For the examples in this paper, TL is calculated with ORCA.[4] This range-independent normal mode model treats the shallow ocean environment as a waveguide with the seabed parameters $\boldsymbol{\theta}$ modeled using acousto-elastic parameters of density, compressional and shear wave speeds and attenuations. ORCA computes the frequency-dependent modal eigenvalues $k_n(f;\boldsymbol{\theta})$ and normalized depth-dependent mode functions $\bar{\phi}_n(z,f;\boldsymbol{\theta})$, where f is the frequency in Hz. From these properties of the waveguide and a specified source and receiver geometry, the Green's function is calculated:

$$p(z_s,z_r,r,f;\boldsymbol{\theta}) \approx \frac{\sqrt{2\pi e^{i\pi/4}}}{\rho_s}\sum_{n=1}^{N}\bar{\phi}_n(z_s,f;\boldsymbol{\theta})\bar{\phi}_n(z_r,f;\boldsymbol{\theta})\frac{e^{ik_n(f;\boldsymbol{\theta})r}}{\sqrt{k_n(f;\boldsymbol{\theta})r}} \tag{2}$$

where $\phi_n(z_s)$ and $\phi_n(z_r)$ are the n-th depth-dependent normal mode functions evaluated at the source depth z_s and receiver depth z_r, respectively; $k_n(f)$ is the n-th modal eigenvalue; ρ_s is the density at the source depth; and r is the horizontal range between source and receiver.

From the Green's function, the frequency-dependent TL is calculated:

$$\mathrm{TL}(z_s,z_r,r,f;\boldsymbol{\theta}) = -20\log_{10}(|p(z_s,z_r,r,f;\boldsymbol{\theta})|). \tag{3}$$

TL has units of dB relative the level 1 m from an acoustic source.

C. VISCOUS GRAIN SHEARING MODEL

While the input parameters to the ORCA model are the acousto-elastic parameters, this work begins with a more fundamental model: a sediment acoustics model known as Buckingham's Viscous Grain Shearing (VGS) model.[1–3] The VGS model serves as a valuable tool, providing physical bounds to the parameter space and offering insights into 1) the frequency dependence of sound speed and attenuation and 2) naturally occurring marine sediments, such as mixtures of clay,

Table 1: Viscous Grain Shearing model parameters. Default values correspond to a sediment type identified as "coarse silt" in Table 2. Min and Max refer to the bounds of the parameter space sampled in generating the model manifold.

Parameter	Name	SI Units	Default Values	Min	Max
N	Porosity	-	0.471	0.372	0.90
N_0	Reference Porosity	-	0.37	-	-
ρ_w	Bottom Water Density	kg/m^3	1023	-	-
K_w	Bottom Water Bulk Modulus	GPa	2.24	-	-
ρ_g	Grain Density	kg/m^3	2550	2500	2650
K_g	Grain Bulk Modulus	GPa	22	8.85	36
μ_0	Reference Grain Diameter	μm	1000	-	-
γ_0	Reference Compressional Modulus	GPa	0.3545	-	-
γ_0	Reference Shear Modulus	GPa	0.0447	-	-
n	Strain Hardening Index	-	0.07	0.045	0.12
τ	VGS Time Constant	s	1.2 E-4	1.2 E-4	1111.0
τ_0	Reference Time Constant	s	1	-	-
z_0	Reference Depth	m	0.3	-	-
T	Sediment Thickness	m	20	-	-

silt, and sand. The VGS model is a causal sediment acoustics model, capable of reasonably treating the broadest range of sediment types.[8] The VGS modeling parameters are listed in Table 1. Some are related to the grains, some to the fluid between the grains, and others are constant reference parameters. The default values for the VGS modeling parameters used in the Results section are also listed in Table 1. From the VGS parametrization of the sediment, the depth-dependent acousto-elastic parameters are calculated using the relationships derived by Buckingham.[1–3]

In this study, we consider a parameter space consisting of five VGS parameters: the sediment layer's porosity N, grain density ρ_g, grain bulk modulus K_g, strain hardening index n, and the visco-elastic time constant τ. These parameters are sampled over the minimum and and maximum values in Table 1, while all other parameters are held constant at the default values. The parameters N, ρ_g, K_g, and n were linearly sampled 50 times, and τ was sampled 50 times with log spacing.

The goal is to explore the parameter space by varying all five VGS parameters, effectively examining a five-dimensional manifold. However, visualizing this high-dimensional space directly is not feasible. Instead, two-dimensional slices of the model manifold are obtained by varying two parameters at a time while keeping the other three parameters fixed at the values in Table 1. Additionally, the following ocean parameters were held constant throughout the investigation: i.e., water depth $h_w = 100$ m, and water sound speed $c_w = 1500$ m/s.

D. DATA SPACE

The ORCA model maps the five-dimensional parameter space to data space. Data space is defined by the number of *observations* or, in this case, the number of source-receiver configura-

Table 2: Examples of VGS parameter values for different sediment types, adapted from Table II of Knobles et al.[9]

Sediment type	N	ρ_g	K_g	n	τ
Granules	0.372	2650	36.0	0.12	1.2 E-4
Very coarse sand	0.374	2650	36.0	0.111	1.2 E-4
Coarse sand	0.378	2650	32.0	0.100	1.2 E-4
Medium sand	0.385	2650	28.0	0.095	1.2 E-4
Fine Sand	0.399	2600	28.0	0.085	1.2 E-4
Very fine sand	0.425	2600	28.0	0.080	1.2 E-4
Coarse silt	0.471	2550	22.0	0.0785	1.2 E-4
Silty sand	0.500	2600	19.0	0.0775	1.2 E-4
Medium silt	0.543	2525	14.67	0.067	1.2 E-2
Clayey sand silt	0.600	2500	13.67	0.065	1111.0
Fine silt	0.640	2500	13.61	0.060	1111.0
Silty clay	0.694	2500	13.55	0.0575	1111.0
Very fine silt	0.735	2500	13.50	0.055	1111.0
Clay	0.750	2500	13.50	0.045	1111.0
Very soft clay	0.90	2500	8.850	0.045	1111.0

tions, at which the modeled $\mathrm{TL}(z_s, z_r, r, f; \boldsymbol{\theta})$ are computed. For the examples in this paper, model manifolds are shown for TL at f=100 Hz with $z_s = 6$ m, and $r = 3$ km. Sixteen receiver depths are defined between $z_r = 40.75$ and 97 m, with a constant spacing of 3.75 m. Thus, the resulting five-dimensional model manifolds are embedded in a 16 dimensional data space.

E. PRINCIPAL COMPONENT ANALYSIS

One approach to visualize N-dimensional model manifolds embedded in a M-dimensional data space ($M > 3$) is to use a principal component analysis (PCA). PCA is a method for finding the directions of greatest variance in a dataset, which correspond to the eigenvectors of the covariance matrix. These eigenvectors are referred to as the *principal components* and represent the axes of a rotated coordinate system that better align with the directions of high variability on the model manifold. When the model manifold is projected onto the principal component axes, the contributions of the first two or three principal components to the model manifold can be plotted to view a large percentage of the structure of the N-dimensional model manifold embedded in the M-dimensional data space. These PCA representations of the five-dimensional model manifold embedded in 16-dimensional data space are shown in the results section.

3. RESULTS

These results highlight two possible ways in which parameter sloppiness/stiffness can be investigated using the model manifolds. First, a PCA representation of the TL model manifold reveals the relative sloppiness of the parameters on the edges of two-dimensional slices of data space. Second, the information distance on the TL model manifold between specific sediment types is calculated in the 16-dimensional data space. Both of these approaches provide evidence that porosity is the stiffest parameter for this case.

A. MODEL MANIFOLDS

To examine the relative stiffness and sloppiness of parameters for our conditions, we performed a principal component analysis (PCA) on the five-dimensional TL model manifold embedded in 16-dimensional data space. We then look at two-dimensional slices of the PCA representation of the TL model manifold, which correspond to varying two of the five parameters. This PCA representation allows for visual inspection of the edges of the model manifold associated with changes in a single parameter.

Examples of these PCA representations of the TL model manifold are shown in Fig. 3. These plots correspond to two-dimensional slices of the model manifold in which porosity N and one other parameter is varied: (a) grain density ρ_g, (b) grain bulk modulus K_g, (c) strain hardening index n, and (d) visco-elastic time constant τ. In all cases, the yellow and purple edges correspond to variations in porosity while the other parameter is held at one of its extrema values from Table 1, and the blue and red edges when porosity is held at its extrema value and the other parameter is varied.

The length of these edges provides insights into the relative sloppiness/stiffness of the five VGS parameters for TL. In Figure 3a, c, and d, the boundaries relating to varying porosity (yellow and purple) are longer than the boundaries corresponding to changes in the the other variable. These longer boundaries imply that porosity is a very stiff parameter: Changes in the value of porosity change the TL significantly more than changes in ρ_g and n generally and K_g and τ in the high porosity limit (red). For lower porosity (blue), variations in K_g and τ correspond to a longer boundary for this TL model manifold.

B. INFORMATION DISTANCES

In addition to looking at the edges of the model manifolds to find sloppy parameters and other trends, the Euclidean distances between points on the five-dimensional model manifold embedded in the 16-dimensional data space can be calculated. The resulting information distances relate to the acoustic distinguishability between specific sediment types corresponding to different modeling parameters. As an example, the TL model manifold at 100 Hz was calculated for 15 sediment types using the values in Table 2. This table is adapted from the one in Knobles *et. al*,[9] with the exception that the roughness parameter of the sediment is not included. The ORCA model maps each of these 15 sediment types to a specific location on the TL model manifold, and the information distance between each pair was calculated (using a 16-dimensional Euclidean distance). The information distances between each pair of sediment types is displayed in Fig. 4.

This matrix provides a visual representation of the difference in TL due to a change in sediment

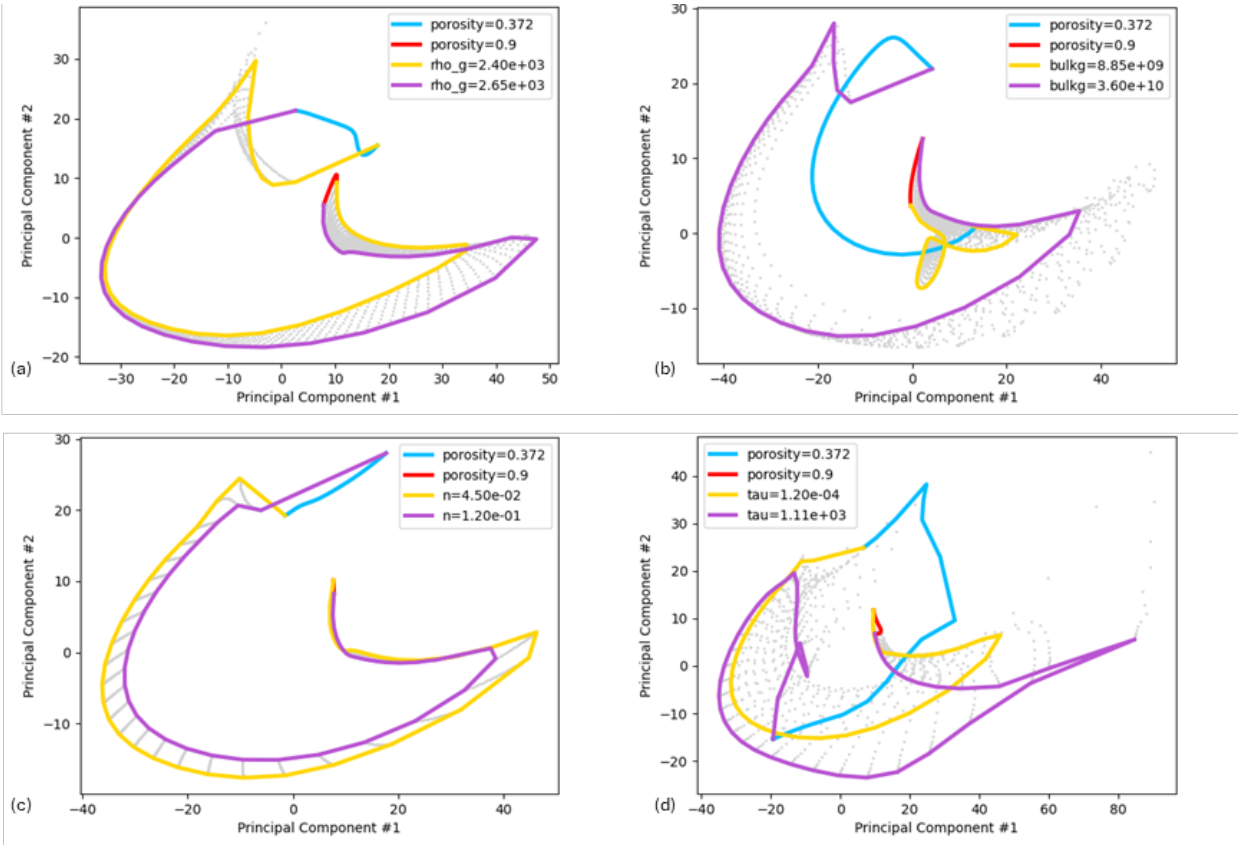

Figure 3: First two principal components from the 16-dimensional data space for two-dimensional slices of the model manifold: (a) Porosity (N) ***vs Grain Density*** (ρ_g)***, (b) Porosity*** (N) ***vs Grain Bulk Modulus*** (K_g)***, (c) Porosity*** (N) ***vs Strain Hardening Index*** (n)***, (d) Porosity*** (N) ***vs VGS Time Constant*** (τ)***. All models are for*** TL ***at*** $f = 100$ ***Hz and*** $r = 3$ ***km, with*** $h_w = 100$ ***m and a single sediment layer with thickness*** $T = 20$ ***m***

types. This approach can be used in experimental design to determine if different sediment types can be distinguished by data at certain frequencies and ranges.

4. CONCLUSION

This paper reports our initial work with TL model manifolds based on the viscous grain shearing (VGS) model of the sediment (Buckingham 2005, 2020) and provides a preliminary estimate of the relative parameter sloppiness. While the VGS model includes many modeling parameters (Table 1), the five parameters related to the grains tend to vary between different sediment types. By varying sets of two VGS parameters over the expected parameter bounds, two-dimensional slices of the model manifold for TL at 16 depths have been evaluated. Beyond the single example shown here, several trends have emerged: 1) model manifolds tend to be narrower for higher frequencies f; 2) model manifolds tend to be more complex (less smooth) at longer source-receiver ranges r; and 3) porosity is the stiffest (most impactful), parameter. These additional studies also show that the length of the model manifold edge associated with porosity are 1) generally longer

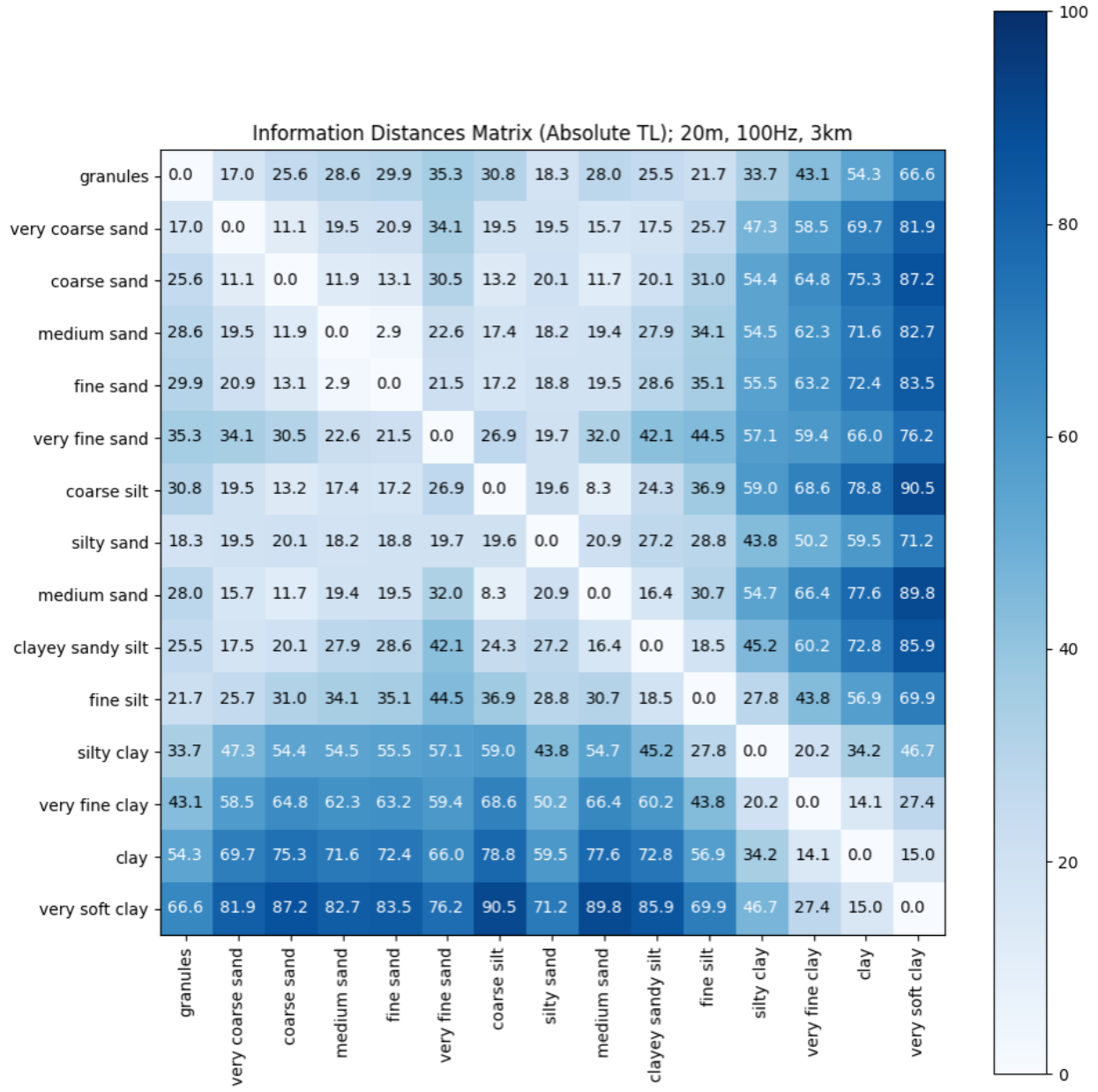

Figure 4: Information Seabed Distances Matrix. The information distance between each of locations on the TL ***model manifold corresponding to each of the sediment types in Table 2 assuming a seabed composed of single sediment layer with thickness*** $=$ ***20 m over a half-space for*** f $=$***100 Hz and*** r $=$***3 km.***

than those corresponding with changes in other variables, 2) slightly dependent on frequency, and 3) significantly larger for propagation ranges greater than 2 km.

Another way to evaluate the five-dimensional model in 16-dimensional data space is to consider the information distance between specific seabed types. Knobles *et. al*[9] proposed a set of 15 VGS sediment types ordered by increasing porosity, which are listed in Table 2. Each of these sets of parameter combinations maps to a single location on the TL model manifold at a specified frequency and range. The information distances between the sediment types (assuming a 20 m sediment layer over a half-space) have been evaluated for the case of $f = 100$ Hz and $r = 3$ km, $z_s = 6$ m, and 16 evenly spaced receivers with $z_r = 40.75 - 97.0$ m. In general, the information distances between the sediment types increase with increasing porosity, which provides additional evidence that porosity is generally the stiffest parameter and likely a good candidate for developing a reduced-order model of the seabed.

ACKNOWLEDGMENTS

This work relates to the Department of the Navy Awards N00014-24-12566 issued by the Office of Naval Research. Any opinions, findings, and conclusions or recommendations expressed in this material are those of the authors and do not necessarily reflect views of the Office of Naval Research. We would like to thank National Science Foundation Grant 2348770 for providing funding for a Research Experience for Undergraduates at Brigham Young University for A. Smith, and undergraduate research assistant funding provided to M. Wang by the College of Computing, Mathematical, and Physical Sciences at Brigham Young University.

REFERENCES

[1] M. J. Buckingham, "Compressional and shear wave properties of marine sediments: Comparisons between theory and data," The Journal of the Acoustical Society of America **117**(1), 137–152 (2005).

[2] M. J. Buckingham, "On pore-fluid viscosity and the wave properties of saturated granular materials including marine sediments," The Journal of the Acoustical Society of America **122**(3), 1486–1501 (2007).

[3] M. J. Buckingham, "Wave speed and attenuation profiles in a stratified marine sediment: Geoacoustic modeling of seabed layering using the viscous grain shearing theory," The Journal of the Acoustical Society of America **148**(2), 962–974 (2020).

[4] E. K. Westwood, C. T. Tindle, and N. R. Chapman, "A normal mode model for acousto-elastic ocean environments," The Journal of the Acoustical Society of America **100**(6), 3631–3645 (1996) 10.1121/1.417226.

[5] C. L. Pekeris, "THEORY OF PROPAGATION OF EXPLOSIVE SOUND IN SHALLOW WATER," in *Geological Society of America Memoirs* (Geological Society of America, 1948), pp. 1–116, 10.1130/mem27-2-p1.

[6] G. V. Frisk, *Chapter 5: The Method of Normal Modes*, 110–163 (P T R Prentice-Hall).

[7] M. J. Buckingham and S. A. S. Jones, "A new shallow-ocean technique for determining the critical angle of the seabed from the vertical directionality of the ambient noise in the water column," The Journal of the Acoustical Society of America **81**(4), 938–946 (1987) 10.1121/1.394573.

[8] C. W. Holland, J. Dettmer, and S. E. Dosso, "Some reflections on buckingham's viscous grain shearing model," The Journal of the Acoustical Society of America **146**(4_Supplement), 2857–2857 (2019).

[9] D. Knobles, T. B. Neilsen, W. S. Hodgkiss, and J. A. Goff, "Inference of source signatures of merchant ships in shallow ocean environments," The Journal of the Acoustical Society of America **155**(5), 3144–3155 (2024).

[10] K. Li and M. Chitre, *24th International Congress on Acoustics*, 37–50.

[11] D. J. Brooker, S. Finette, and P. C. Mignerey, "Detection on a distributed network using information geometry," JASA Express Letters **1**(3), 036001 (2021) 10.1121/10.0003617.

[12] S. Finette and P. C. Mignerey, "Stochastic matched-field localization of an acoustic source based on principles of riemannian geometry," The Journal of the Acoustical Society of America **143**(6), 3628–3638 (2018) 10.1121/1.5040492.

[13] N. R. Chapman and E. C. Shang, "Review of geoacoustic inversion in underwater acoustics," Journal of Theoretical and Computational Acoustics **29**(03) (2021) 10.1142/s259172852130004x.

[14] J. Nuttall, "Maximum entropy approach to bayesian inference of geoacoustic and source parameters using sound from transiting ships" (2023) undergraduate Senior Thesis, Brigham Young University.

[15] E. K. Westwood and R. A. Koch, "Elimination of branch cuts from the normal-mode solution using gradient half spaces," The Journal of the Acoustical Society of America **106**(5), 2513–2523 (1999) 10.1121/1.428083.

[16] M. K. Transtrum and P. Qiu, "Model reduction by manifold boundaries," Physical Review Letters **113**(9) (2014) 10.1103/physrevlett.113.098701.

[17] M. C. Mortenson, T. B. Neilsen, M. K. Transtrum, and D. P. Knobles, "Accurate broadband gradient estimates enable local sensitivity analysis of ocean acoustic models," Journal of Theoretical and Computational Acoustics (2023) 10.1142/s2591728522500153.

[18] F. B. Jensen, W. A. Kuperman, M. B. Porter, and H. Schmidt, *Computational Ocean Acoustics*, 2nd ed. (Springer, 2011).

[19] J. Gebbie and M. Siderius, "Optimal environmental estimation with ocean ambient noise," The Journal of the Acoustical Society of America **149**(2), 825–834 (2021) 10.1121/10.0003353.

[20] M. Siderius and J. Gebbie, "Environmental information content of ocean ambient noise," The Journal of the Acoustical Society of America **146**(3), 1824–1833 (2019) 10.1121/1.5126520.

[21] A. Baggeroer and H. Schmidt, "Cramer-rao bounds for matched field tomography and ocean acoustic tomography," in *1995 International Conference on Acoustics, Speech, and Signal Processing*, IEEE (1995), 10.1109/icassp.1995.479417.

[22] S. R. Tuladhar and J. R. Buck, "Optimum array design to maximize fisher information for bearing estimation," The Journal of the Acoustical Society of America **130**(5), 2797–2806 (2011) 10.1121/1.3644914.

[23] A. B. Baggeroer, W. A. Kuperman, and H. Schmidt, "Matched field processing: Source localization in correlated noise as an optimum parameter estimation problem," The Journal of the Acoustical Society of America **83**(2), 571–587 (1988) 10.1121/1.396151.

[24] M. Mortenson, "Physics-guided machine learning in ocean acoustics using fisher information," Master's thesis (2022).

[25] S. C. Walker, C. Yardim, A. Thode, and E. Arias-Castro, "Using fisher information to quantify uncertainty in environmental parameters estimated from correlated ambient noise," The Journal of the Acoustical Society of America **133**(4), EL228–EL234 (2013) 10.1121/1.4792836.

[26] M. K. Transtrum, A. T. Saric, and A. M. Stankovic, "Measurement-directed reduction of dynamic models in power systems," IEEE Transactions on Power Systems **32**(3), 2243–2253 (2017) 10.1109/tpwrs.2016.2611511.

[27] C. C. Youn, A. T. Saric, M. K. Transtrum, and A. M. Stankovic, "Information geometry for model reduction of dynamic loads in power systems," in *2017 IEEE Manchester PowerTech*, IEEE (2017), 10.1109/ptc.2017.7981280.

[28] M. K. Transtrum, B. L. Francis, A. T. Saric, and A. M. Stankovic, "Simultaneous global identification of dynamic and network parameters in transient stability studies," in *2018 IEEE Power &amp Energy Society General Meeting (PESGM)*, IEEE (2018), 10.1109/pesgm.2018.8586586.

[29] G. L. Marschmann, H. Pagel, P. Kügler, and T. Streck, "Equifinality, sloppiness, and emergent structures of mechanistic soil biogeochemical models," Environmental Modelling &amp Software **122**, 104518 (2019) 10.1016/j.envsoft.2019.104518.

[30] M. Imbrišak and K. Nomura, "Stability of the manifold boundary approximation method for reductions of nuclear structure models," Physical Review C **107**(3) (2023) 10.1103/physrevc.107.034304.

[31] C. Petrie, C. Anderson, C. Maekawa, T. Maekawa, and M. K. Transtrum, "The supremum principle selects simple, transferable models" (2021), 10.48550/ARXIV.2109.10449.

[32] H. Yang, K. Lee, Y. Choo, and K. Kim, "Underwater acoustic research trends with machine learning: general background," Journal of Ocean Engineering and Technology **34**(2), 147–154 (2020).

[33] D. F. V. Komen, T. B. Neilsen, K. Howarth, D. P. Knobles, and P. H. Dahl, "Seabed and range estimation of impulsive time series using a convolutional neural network," The Journal of the Acoustical Society of America **147**(5), EL403–EL408 (2020) 10.1121/10.0001216.

[34] D. F. Van Komen, T. B. Neilsen, D. B. Mortenson, M. C. Acree, D. P. Knobles, M. Badiey, and W. S. Hodgkiss, "Seabed type and source parameters predictions using ship spectrograms in convolutional neural networks," The Journal of the Acoustical Society of America **149**(2), 1198–1210 (2021).

[35] J. C. Spendlove, T. B. Neilsen, and M. K. Transtrum, "Information geometry analysis example for absolute and relative transmission loss in a shallow ocean," JASA Express Letters **4**(7) (2024) 10.1142/S2591728524500117.

[36] W. M. Sanders and M. D. Richardson, "Parameter estimation errors in buckingham's grain shearing model," in *OCEANS 2009* (2009), pp. 1–8, 10.23919/OCEANS.2009.5422390.

[37] A. Anu, P. V. Nair, C. Uthaman, and T. P. Kumar, "Estimation of compressional wave speed in marine sediments using biot-stoll model and buckingham's grain-shearing model," Defence Science Journal **70**(3), 336–341 (2020).